ACS APPLIED ELECTRONIC MATERIALS

pubs.acs.org/acsaelm Letter

Local Atomic Configuration Control of Superconductivity in the Undoped Pnictide Parent Compound $BaFe_2As_2$

Jong-Hoon Kang, Philip J. Ryan, Jong-Woo Kim, Jonathon Schad, Jacob P. Podkaminer, Neil Campbell, Joseph Suttle, Tae Heon Kim, Liang Luo, Di Cheng, Yesusa G. Collantes, Eric E. Hellstrom, Jigang Wang, Robert McDermott, Mark S. Rzchowski, and Chang-Beom Eom*

Cite This: *ACS Appl. Electron. Mater.* 2022, 4, 1511−1517 Read Online

ACCESS | Metrics & More | Article Recommendations | Supporting Information

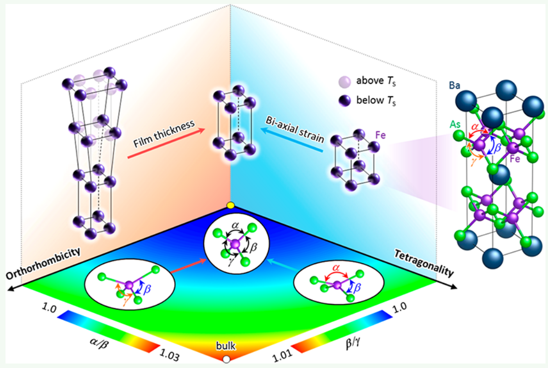

ABSTRACT: Emergent superconductivity is strongly correlated with the symmetry of local atomic configuration in the parent compounds of iron-based superconductors. While chemical doping or hydrostatic pressure can change the local geometry, conventional approaches do not provide a clear pathway in predictably tuning the detailed atomic arrangement due to the parent compound's complicated structural deformation in the presence of the tetragonal-to-orthorhombic phase transition. Here, we demonstrate a systematic approach to manipulate local structural configurations in $BaFe_2As_2$ epitaxial thin films by controlling two independent structural factors, orthorhombicity (in-plane anisotropy) and tetragonality (out-of-plane/in-plane balance), from lattice parameters. We tune superconductivity without doping utilizing both structural factors separately and controlling local tetrahedral coordination in the designed thin film heterostructures with substrate clamping and biaxial strain. We further show this allows quantitative control of the structural phase transition, the associated magnetism, and superconductivity in parent material $BaFe_2As_2$. This approach will advance the development of tunable thin film superconductors in a reduced dimension.

KEYWORDS: *superconductivity, thin films, atomic configuration, phase transition, parent materials*

A pervasive issue affecting the fundamental understanding and practical application of high temperature superconductors is the identification of the factors that determine the maximum critical temperature ($T_{c,max}$) for a given material family. In the case of Fe-based superconductors, the attention has primarily focused on the inter-relation between superconductivity and other broken-symmetry phases found in the phase diagram, principally magnetic order.[1−8] Even though the physical origin of the symmetry-breaking ground state remains controversial, structural factors, possibly associated with the above relationship, have been shown to play an important role in determining $T_{c,max}$ and broken symmetries.[9−17] Several early investigations of a variety of optimally doped, tetragonal, and bulk Fe−pnictide superconductors revealed an apparent correlation between $T_{c,max}$ and the proximity to perfect tetrahedral coordination of the Fe ions, which can control effective hopping parameters for electrons moving in the associated Fe−As planes.[18−20] For underdoped compositions, however, the presence of a tetragonal-to-orthorhombic phase transition makes it considerably more difficult to assess the impact of these structural effects on T_c.

Structural distortions and superconductivity have been induced in the undoped pnictide parent compound by either chemical substitution or the application of high hydrostatic pressure.[9,21−25] It has been suggested that emergent superconductivity may be associated with local or global strains that change the local atomic structure, affecting the tetrahedral bond angles α, β, and γ. However, these external stimuli do not provide an ideal approach to assess the relative roles played by structural distortions and associated structure−property relations because the internal distortion of the tetrahedral geometry is not predictable. A desired approach is to determine the orthogonal factors to suppress the orthorhombic distortion and change the tetragonal unit cell independently and, hence, control the detailed bond angles of subunit cell structures in the parent material.

Here, we use epitaxial strain in designed thin film heterostructures to control crystal symmetry such as in-plane (orthorhombicity) and in-plane/out-of-plane anisotropies (tetragonality), and by doing so, the sublattice structure can

Received: March 3, 2022
Accepted: March 23, 2022
Published: March 31, 2022

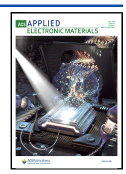

Downloaded via FLORIDA STATE UNIV on March 4, 2026 at 18:15:42 (UTC).
See https://pubs.acs.org/sharingguidelines for options on how to legitimately share published articles.

ACS Publications © 2022 American Chemical Society

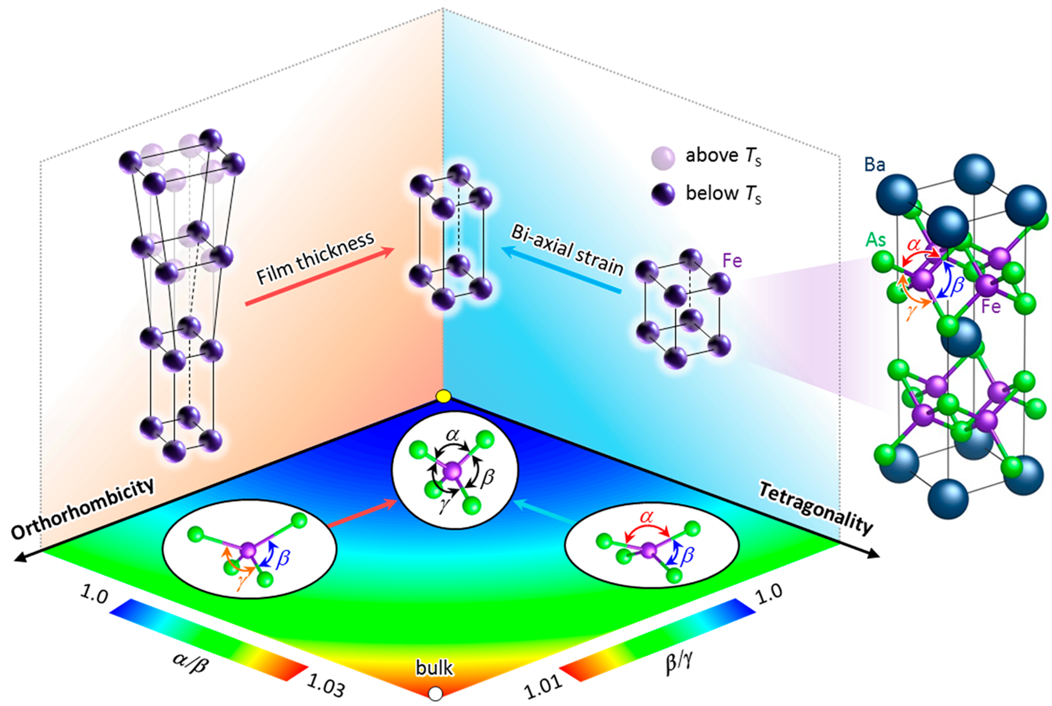

Figure 1. Schematic picture of the structural design in parent Fe-based compounds. Individual control of orthorhombicity and tetragonality determines lattice stability toward or away from the perfect tetrahedral geometry in the presence of the tetragonal-to-orthorhombic transition. Each decoupled parameter is tuned by film thickness and biaxial strain, independently. Orthorhombic transition below T_s is more suppressed in the thinner film by the substrate clamping effect, and tetragonality is modified by in-plane strain. Orthorhombicity and tetragonality control anisotropy between angles β and γ and between α and β, respectively, and a perfect tetrahedron can be obtained by reducing structural anisotropy under the control of orthorhombicity and tetragonality.

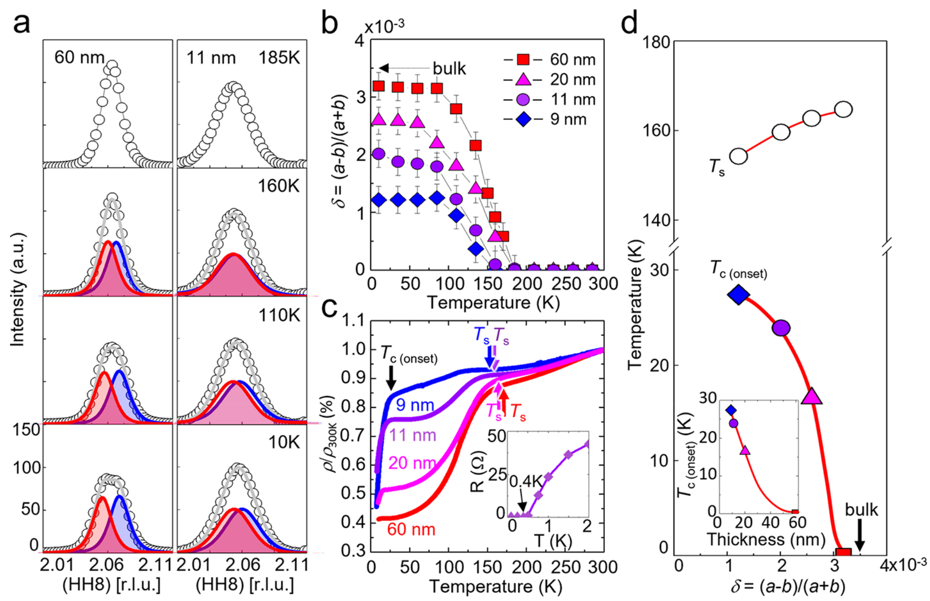

Figure 2. Superconductivity enhanced by suppression of orthorhombic phases. (a) Tetragonal-to-orthorhombic structural change along the [hh8] direction across the tetragonal (228) reflection by X-ray diffraction at different film thickness. All films were grown on LiF substrates at 680 °C. (b) Temperature-dependent orthorhombicity δ extracted from (228) reflections. (c) Normalized resistivity as a function of temperature for different film thicknesses. The inset (11 nm, LiF substrate) shows a full superconducting transition with zero resistance at 0.4 K. (d) Superconducting T_c and structural phase transition (T_s) correlated with δ (taken at 10 K). Note that c/a is fixed as 3.348 below T_s. T_c as a function of film thickness shown in the inset. Red lines are guides to the eye.

be precisely manipulated. For this, the nominally non-superconducting parent compound $BaFe_2As_2$ (Ba-122) is utilized to grow epitaxial thin films on different substrates[26] with different film thicknesses[15] and correlate changes in T_c with structural factors. The structural control of Ba-122 thin films was through the epitaxial relationship of the film with the substrate (see the Supporting Methods and Figure S1) based on the study of atomic configurations and their concomitant

https://doi.org/10.1021/acsaelm.2c00291
ACS Appl. Electron. Mater. 2022, 4, 1511−1517

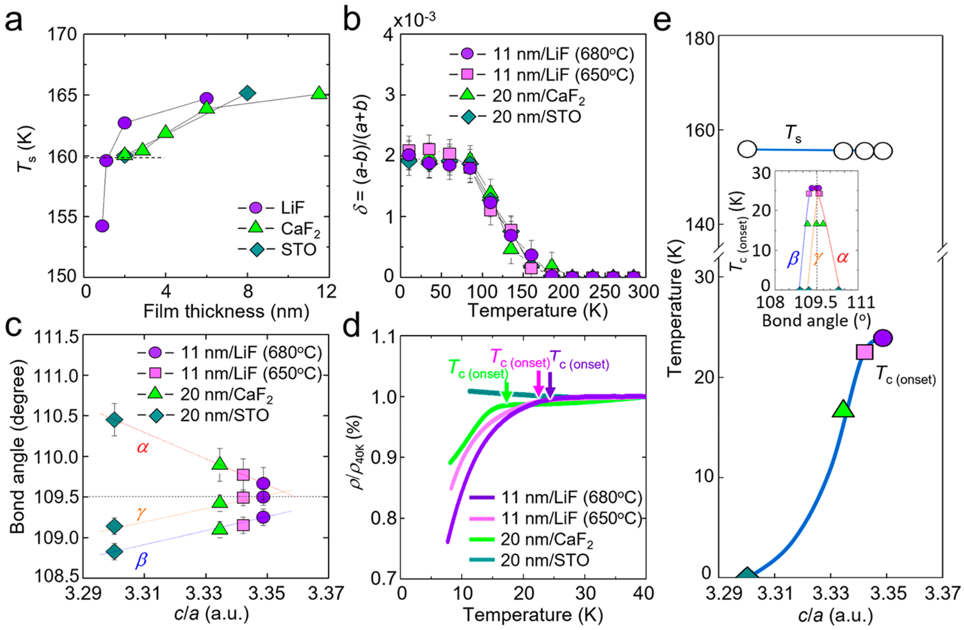

Figure 3. Superconductivity tuned by tetragonal structures. (a) Thickness-dependent T_s in different substrates. The growth temperature on LiF is 680 °C. (b) Identical temperature-dependent δ of films with the same T_s. (c) As−Fe−As bond angles α, β, and γ in a tetrahedron controlled by the c/a ratio. (d) Normalized resistivity showing different onsets of T_c. (e) T_c and T_s as a function of tetragonality (c/a taken at 10 K). T_c as a function of bond angles shown in the inset. Blue line is a guide to the eye.

dead layers at the interfaces.[26] As indicated schematically in Figure 1, we employ two strategies to control the degree of tetragonality c/a above the structural phase transition (which occurs at a temperature T_s), and the orthorhombicity $\delta = (a - b)/(a + b)$ for temperatures below T_s. First, different cubic substrates ($SrTiO_3$, CaF_2, and LiF) and growth conditions directly tune c/a above T_s without breaking any symmetry. Second, when films with different thicknesses are grown, the degree of orthorhombicity δ below T_s is effectively tuned. In particular, for very thin films, δ is suppressed due to a "clamping" effect arising from epitaxy with the cubic substrate. This relaxes as the film thickness is increased (approaching a free-standing bulk crystal), leading to larger values of δ for thicker films. Hence, substrate type and film thickness provide controls of the As−Fe−As bond angles α, β, and γ even in the orthorhombic phase.

■ RESULTS

Influence of Orthorhombicity and Tetragonality. Tetragonality and orthorhombicity provide a straightforward way to manipulate bond angles (Figure 1). In the tetragonal structure above T_s, there are only two unique bond angles: α and $\beta = \gamma$ (see the Supporting Methods). In the orthorhombic state below T_s, β differs from γ as a result of broken rotational symmetry arising from anisotropy of the in-plane lattice constants. The bond angle α is associated with the next-nearest-neighbor interaction of Fe 3d orbitals, while β and γ are linked with nearest-neighbor hopping, which determines the antiferromagnetic ordering[19,27] (see Figure S2). We control these bond angles as well as the electronic and magnetic properties with film tetragonality and orthorhombicity.

Control of Orthorhombic Distortion by the Clamping Effect. Figure 2 shows that superconductivity can be enhanced by the suppression of orthorhombicity. High-resolution synchrotron XRD demonstrates that a single sharp peak is observed above the structural transition temperature T_s in Figure 2a. Regardless of film thickness, growing films on LiF substrates results in identical sharp peak positions for temperatures just above T_s (∼160 K), which implies constant tetragonal lattice parameters of the films. Upon cooling below T_s, the (228) reflection is broadened with a peak intensity drop due to peak splitting associated with the orthorhombic transition as observed in bulk.[28,29] The splitting is temperature dependent, increasing with decreasing temperature until reaching a low-temperature plateau. Its overall magnitude is reduced in thinner films due to substrate clamping. We perform fitting on the XRD data to determine the structural factor of orthorhombicity, $\delta = (a - b)/(a + b)$, and use its low-temperature plateau value to quantitatively compare between films and correlate the structural information with electronic properties (see the Supporting Methods). Figure 2b shows the temperature-dependent δ with a transition to the low-temperature plateau that is broader in these thin films than in bulk crystals.[6] The overall reduction of δ with decreasing film thickness is clearly shown. The low-temperature saturated δ value is reduced, and the onset of orthorhombicity is shifted to a lower temperature as film thickness is reduced.[30]

As shown in Figure 2b,c, there is a resistive anomaly near the orthorhombic structural transition. We assign T_s to the onset of the upturn in the first derivative of the resistivity with respect to temperature ($d\rho/dT$) and use this value to characterize the orthorhombic transition (see Figure S3). This provides a more precise comparison temperature than that obtained from the XRD data. We confirmed that the onset of orthorhombic δ is consistent with this resistive T_s (Figure 2b), as in bulk materials.[29−31] The structural transition measured by the orthorhombicity shows a broad temperature dependence, unlike the near first order transition observed in Ba-122 single crystals.[29−31] We probe the magnetic phase transition temperature (T_n) with reflection optical polarimetry[32] (see the Supporting Methods). Here, the measured

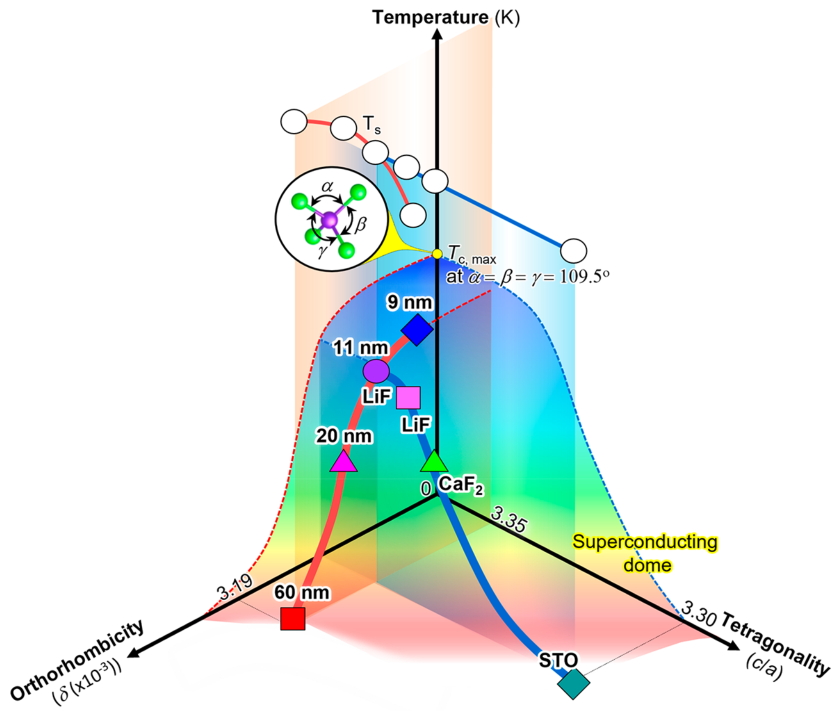

Figure 4. Three-dimensional phase diagram of parent $BaFe_2As_2$ materials. Demonstration of explicit guidelines showing how to enhance T_c with the existence of the tetragonal-to-orthorhombic transition. Decoupling the two structural parameters of orthorhombicity and tetragonality is the key for approaching the ideal tetrahedron where the three bond angles are identical (yellow dot). Solid red and blue lines are drawn from the measured superconducting T_c under the independent control of orthorhombicity and tetragonality.

ellipticity signal, which arises from the 2-fold in-plane anisotropy of the refractive index, sets in below T_s, consistent with the emergence of orthorhombicity, and exhibits a kink at T_n due to the magnetic feedback effect,[32] indicating the relation to the antiferromagnetic transition. T_n does not coincide with T_s in our undoped films as shown in anisotropic characteristics revealed by ellipticity and structural orthorhombicity measurements[33] (see Figure S4c), similar to the behavior of the electron doped parent compound.[34,35]

Control of the Tetragonal Structure with Biaxial Strain. Strain-controlled tetragonality is another structural factor that controls bond angles. As the c/a ratio is increased by compressive strain, bond angles α and β change linearly and approach a single value (Figure 3c). Note that we need to consider the bond angle γ as well because orthorhombicity is not completely suppressed. We control the c/a by film strain, and As−Fe−As bond angles are systematically controlled by the c/a ratio, approaching the optimal angle of 109.5°.

Since the clamping effect differs on each substrate, the same orthorhombicity for films of differing tetragonality can be obtained by varying the film thickness. This allows the separation of effects due to tetragonality and orthorhombicity. We confirmed a set of films on different substrates with identical orthorhombicity but varying tetragonality through measurements of temperature-dependent δ (Figure 3a,b). The out-of-plane lattice constant varies in this set, determined by the in-plane lattice constants through elasticity. Thus, substrate clamping provides tetragonality control through the substrate in-plane lattice constant. For instance, X-ray diffraction confirms that Ba-122 films grown on dissimilar substrates have different in-plane lattice constants and also different tetragonality (c/a) due to the film strain. In particular, fluoride substrates provide more compressive strain than oxides due to higher thermal contraction and the resulting thermal strain.

Influence of Controlled Structural Distortions on T_s and T_c. We have demonstrated that tetragonality and orthorhombicity can be controlled in the undoped $BaFe_2As_2$. Here, we show that these structural distortions determine the orthorhombic structural phase transition temperature T_s and the superconducting phase transition temperature T_c, inducing superconductivity in this undoped parent compound. These results are summarized in Figures 2d and 3e. Normalized resistivity of individual samples shows a distinct superconducting transition, and the onset of T_c is obtained from the resistivity curve (Figure 3d). Note that, as discussed above, the 11 nm thick Ba-122 film grown on LiF at 680 °C has zero resistance at 0.4 K (inset of Figure 2c).

Figure 3e shows that superconductivity with an onset temperature as high as 27 K can be induced by a suppression of orthorhombicity by substrate clamping at low thickness. Figure 2d shows that films of fixed orthorhombicity but different tetragonality have the same T_s but dramatically varying T_c. We can summarize our results in terms of orthorhombicity, tetragonality, orthorhombic structural phase transition temperature T_s, and superconducting phase transition temperature T_c. In the range we investigated, tetragonality enhances superconductivity and orthorhombicity degrades superconductivity. Tetragonality does not strongly influence T_s, while orthorhombicity correlates with an increase in T_s. Although structural deformations and their interaction with each other, with electronic and magnetic properties, and with spatial gradients can be quite complex, our results point to clear correlations. We have shown that the reduction of in-plane lattice anisotropy (a and b) increases the superconducting transition temperature.

https://doi.org/10.1021/acsaelm.2c00291
ACS Appl. Electron. Mater. 2022, 4, 1511−1517

The constant T_s in films with varying tetragonality but identical orthorhombicity is reflective of the nematic transition driven by either a spin or orbital mechanism. If a spin or orbital mechanism drives the nematic transition, its essential coupling to the orthorhombic structural distortion would connect a larger low-temperature orthorhombicity with a stronger nematicity and associated higher transition temperature. We argue that the dependence of superconducting T_c on both orthorhombicity and tetragonality is related to the Fe−As bond angles. We found T_c is enhanced by the proximity to all bond angles approaching 109.5° (inset of Figure 3e). Despite lacking experimental realization of perfect 109.5° tetrahedral angles, we have shown that the reduction of asymmetry between α and β (or γ) enhances the superconducting T_c.

Superconductivity emerges as reduced film thickness decreases orthorhombicity, which to our knowledge has not been previously reported on insulating substrates. The enhancement of T_c is tuned by the film thickness due to the substrate clamping effect (inset of Figure 2d). The film with the smallest orthorhombicity becomes fully superconducting with zero resistance, as shown in the inset of Figure 2c (see Figure S5). T_s and onset T_c (due to the broad transition) were plotted as functions of δ to show the correlation of the orthorhombicity factor (δ) with the superconducting T_c (Figure 2d). It is intriguing to see that the reduction of δ is correlated to lower T_s and higher T_c.

Visualizing the Parent Ba-122 Phase Diagram. Although our films do not cover the complete range of single-phase structural distortions, we visualize a phase diagram of parent Ba-122 that guides the manipulation of the As−Fe−As configuration by controlling two separate structural variables (Figure 4). With the designed heterostructures, the selection of substrate templates and film thickness enables one to individually control the parameters to achieve the desired structures. The phase diagram summarizes that decoupled structural factors describing tetrahedral geometry can be systematically controlled so that superconductivity emerges in parent Ba-122. Superconductivity is enhanced by reducing broken symmetry phases as orthorhombicity decreases due to clamping (along the red line) and by approaching a regular tetrahedral coordination as compressive strain tunes tetragonality (along the blue line).

CONCLUSIONS

We experimentally demonstrate a systematic approach to precisely control tetrahedral atomic configurations in parent compounds of Fe-based superconductors through the control of the independent structural factors: orthorhombicity and tetragonality. Our observations are quantitatively explained using atomic-scale detailed structures and concomitant superconducting properties in the thin film heterostructures. This confirms our structural approach is applicable to induce and enhance the superconductivity in ultrathin films without chemical doping in a predictable way. A pure monolayer FeSe with our designed heterostructures would be a good platform to further probe structure−property relationships and to explore unconventional superconductivity in low-dimensional heterostructure films.[36,37] Further, our ultrathin $BaFe_2As_2$ films could break new ground in nonequilibrium materials discovery using terahertz electromagnetic radiation in the superconducting[38,39] and nematic states.[40] We believe our study will provide a path toward tunable low-dimensional superconductivity by atomic structure design.

ASSOCIATED CONTENT

Supporting Information

The Supporting Information is available free of charge at https://pubs.acs.org/doi/10.1021/acsaelm.2c00291.

Methods; X-ray diffraction; temperature-dependent electrical transport; ultrafast time-resolved polarimetry measurement; atomic-resolution synchrotron X-ray diffraction; resonant scattering (PDF)

AUTHOR INFORMATION

Corresponding Author

Chang-Beom Eom − *Department of Materials Science and Engineering, University of Wisconsin-Madison, Madison, Wisconsin 53706, United States;* orcid.org/0000-0002-8854-1439; Email: eom@engr.wisc.edu

Authors

Jong-Hoon Kang − *Department of Materials Science and Engineering, University of Wisconsin-Madison, Madison, Wisconsin 53706, United States;* orcid.org/0000-0002-5109-8402

Philip J. Ryan − *Advanced Photon Source, Argonne National Laboratory, Argonne, Illinois 60439, United States; School of Physical Sciences, Dublin City University, Dublin, Ireland*

Jong-Woo Kim − *Advanced Photon Source, Argonne National Laboratory, Argonne, Illinois 60439, United States*

Jonathon Schad − *Department of Materials Science and Engineering, University of Wisconsin-Madison, Madison, Wisconsin 53706, United States*

Jacob P. Podkaminer − *Department of Materials Science and Engineering, University of Wisconsin-Madison, Madison, Wisconsin 53706, United States*

Neil Campbell − *Department of Physics, University of Wisconsin-Madison, Madison, Wisconsin 53706, United States*

Joseph Suttle − *Department of Physics, University of Wisconsin-Madison, Madison, Wisconsin 53706, United States*

Tae Heon Kim − *Department of Materials Science and Engineering, University of Wisconsin-Madison, Madison, Wisconsin 53706, United States*

Liang Luo − *Department of Physics and Astronomy, Ames Laboratory, Iowa State University, Ames, Iowa 50011, United States*

Di Cheng − *Department of Physics and Astronomy, Ames Laboratory, Iowa State University, Ames, Iowa 50011, United States*

Yesusa G. Collantes − *Applied Superconductivity Center, National High Magnetic Field Laboratory, Florida State University, Tallahassee, Florida 32310, United States*

Eric E. Hellstrom − *Applied Superconductivity Center, National High Magnetic Field Laboratory, Florida State University, Tallahassee, Florida 32310, United States*

Jigang Wang − *Department of Physics and Astronomy, Ames Laboratory, Iowa State University, Ames, Iowa 50011, United States;* orcid.org/0000-0002-6159-4119

Robert McDermott − *Department of Physics, University of Wisconsin-Madison, Madison, Wisconsin 53706, United States*

Mark S. Rzchowski − *Department of Physics, University of Wisconsin-Madison, Madison, Wisconsin 53706, United States*

Complete contact information is available at:
https://pubs.acs.org/10.1021/acsaelm.2c00291

Author Contributions

J.-H.K. and C.-B.E. conceived the project. C.-B.E., M.S.R., R.M., J.W., and E.E.H. supervised the experiments. J.-H.K. synthesized the samples and carried out the X-ray diffraction and transport measurements. J.-H.K., P.J.R., and J.-W.K. performed synchrotron X-ray diffraction and resonant scattering. J.S., J.P.P., and T.H.K. helped with the synchrotron experiments. N.C., J.S., M.S.R., and R.M. carried out the transport measurements. L.L., DC., and J.W. performed laser-based polarimetry to measure ultrafast ellipticity signals. Y.G.C. and E.E.H. prepared PLD targets for the thin film growth. J.-H.K. and C.-B.E. wrote the manuscript. C.-B.E. directed the research.

Notes

The authors declare no competing financial interest.

■ ACKNOWLEDGMENTS

This work was supported by the US Department of Energy (DOE), Office of Science, Office of Basic Energy Sciences (BES), under award number DE-FG02-06ER46327 (C.-B.E.). This research used resources of the Advanced Photon Source, a U.S. Department of Energy (DOE) Office of Science User Facility operated for the DOE Office of Science by Argonne National Laboratory under Contract No. DE-AC02-06CH11357. The synchrotron X-ray diffraction work was partially supported by NSF through the University of Wisconsin Materials Research Science and Engineering Center (DMR-1720415). The work at NHMFL was supported under NSF Cooperative Agreement DMR-1644779 and by the State of Florida. The optical polarimetry work (L.L., D.C., and J.W.) was supported by the U.S. Department of Energy, Office of Basic Energy Science, Division of Materials Sciences and Engineering (Ames Laboratory is operated for the U.S. Department of Energy by Iowa State University under Contract No. DE-AC02-07CH11358). We thank Ian Fisher for helpful discussions.

■ REFERENCES

(1) Fernandes, R. M.; Chubukov, A. V.; Schmalian, J. What drives nematic order in iron-based superconductors? *Nat. Phys.* **2014**, *10*, 97−104.

(2) Fernandes, R. M.; Schmalian, J. Manifestations of nematic degrees of freedom in the magnetic, elastic, and superconducting properties of the iron pnictides. *Supercond. Sci. Technol.* **2012**, *25*, 084005.

(3) Kretzschmar, F.; Böhm, T.; Karahasanović, U.; Muschler, B.; Baum, A.; Jost, D.; Schmalian, J.; Caprara, S.; Grilli, M.; Di Castro, C.; Analytis, J. G.; Chu, J. H.; Fisher, I. R.; Hackl, R. Critical spin fluctuations and the origin of nematic order in $Ba(Fe_{1-x}Co_x)_2As_2$. *Nat. Phys.* **2016**, *12*, 560−563.

(4) Wang, F.; Lee, D.-H. The electron-pairing mechanism of iron-based superconductors. *Science* **2011**, *332*, 200−204.

(5) Kasahara, S.; Shi, H. J.; Hashimoto, K.; Tonegawa, S.; Mizukami, Y.; Shibauchi, T.; Sugimoto, K.; Fukuda, T.; Terashima, T.; Nevidomskyy, A. H.; Matsuda, Y. Electronic nematicity above the structural and superconducting transition in $BaFe_2(As_{1-x}P_x)_2$. *Nature* **2012**, *486*, 382−385.

(6) Cano, A.; Civelli, M.; Eremin, I.; Paul, I. Interplay of magnetic and structural transitions in iron-based pnictide superconductors. *Phys. Rev. B* **2010**, *82*, 020408R.

(7) Chu, J.-H.; Kuo, H.-H.; Analytis, J. G.; Fisher, I. R. Divergent nematic susceptibility in an iron arsenide superconductor. *Science* **2012**, *337*, 710−712.

(8) Onari, S.; Yamakawa, Y.; Kontani, H. High-T_c superconductivity near the anion height instability in Fe-based superconductors: Analysis of $LaFeAsO_{1-x}H_x$. *Phys. Rev. Lett.* **2014**, *112*, 187001.

(9) Kimber, S. A. J.; Kreyssig, A.; Zhang, Y. Z.; Jeschke, H. O.; Valentí, R.; Yokaichiya, F.; Colombier, E.; Yan, J.; Hansen, T. C.; Chatterji, T.; Mcqueeney, R. J.; Canfield, P. C.; Goldman, A. I.; Argyriou, D. N. Similarities between structural distortions under pressure and chemical doping in superconducting $BaFe_2As_2$. *Nat. Mater.* **2009**, *8*, 471−475.

(10) Okabe, H.; Takeshita, N.; Horigane, K.; Muranaka, T.; Akimitsu, J. Pressure-induced high-T_c superconducting phase in FeSe: Correlation between anion height and T_c. *Phys. Rev. B* **2010**, *81*, 205119.

(11) Zhao, J.; Huang, Q.; De La Cruz, C.; Li, S.; Lynn, J. W.; Chen, Y.; Green, M. A.; Chen, G. F.; Li, G.; Li, Z.; Luo, J. L.; Wang, N. L.; Dai, P. Structural and magnetic phase diagram of $CeFeAsO_{1-x}F_x$ and its relation to high-temperature superconductivity. *Nat. Mater.* **2008**, *7*, 953−959.

(12) Paglione, J.; Greene, R. L. High temperature superconductivity in iron-based materials. *Nat. Phys.* **2010**, *6*, 645−658.

(13) Lee, C. H.; Iyo, A.; Eisaki, H.; Kito, H.; Fernandez-Diaz, M. T.; Ito, T.; Kihou, K.; Matsuhata, H.; Braden, M.; Yamada, K. Effect of structural parameters on superconductivity in fluorine-free $LnFeAsO_{1-y}$. *J. Phys. Soc. Jpn.* **2008**, *77*, 083704.

(14) Mizuguchi, Y.; Hara, Y.; Deguchi, K.; Tsuda, S.; Yamaguchi, T.; Takeda, K.; Kotegawa, H.; Tou, H.; Takano, Y. Anion height dependence of T_c for the Fe-based superconductor. *Supercond. Sci. Technol.* **2010**, *23*, 054013.

(15) Kang, J. H.; Kim, J.-W.; Ryan, P. J.; Xie, L.; Guo, L.; Sundahl, C.; Schad, J.; Campbell, N.; Collantes, Y. G.; Hellstrom, E. E.; Rzchowski, M. S.; Eom, C. B. Superconductivity in undoped $BaFe_2As_2$ by tetrahedral geometry design. *Proc. Natl. Acad. Sci. U.S.A.* **2020**, *117*, 21170−21174.

(16) Vaswani, C.; Kang, J. H.; Mootz, M.; Luo, L.; Yang, X.; Sundahl, C.; Cheng, D.; Huang, C.; Kim, R. H. J.; Liu, Z.; Collantes, Y. G.; Hellstrom, E. E.; Perakis, I. E.; Eom, C. B.; Wang, J. Light quantum control of persisting Higgs modes in iron-based superconductors. *Nat. Commun.* **2021**, *12*, 258.

(17) Engelmann, J.; Grinenko, V.; Chekhonin, P.; Skrotzki, W.; Efremov, D. V.; Oswald, S.; Iida, K.; Hühne, R.; Hänisch, J.; Hoffmann, M.; Kurth, F.; Schultz, L.; Holzapfel, B. Strain induced superconductivity in the parent compound $BaFe_2As_2$. *Nat. Commun.* **2013**, *4*, 2877.

(18) Lee, C.-C.; Yin, W.-G.; Ku, W. Ferro-orbital order and strong magnetic anisotropy in the parent compounds of iron-pnictide superconductors. *Phys. Rev. Lett.* **2009**, *103*, 267001.

(19) Han, M. J.; Yin, Q.; Pickett, W. E.; Savrasov, S. Y. Anisotropy, itineracy, and magnetic frustration in high-T_c iron pnictides. *Phys. Rev. Lett.* **2009**, *102*, 107003.

(20) Lv, W.; Wu, J.; Phillips, P. Orbital ordering induces structural phase transition and the resistivity anomaly in iron pnictides. *Phys. Rev. B* **2009**, *80*, 224506.

(21) Rotter, M.; Tegel, M.; Johrendt, D. Superconductivity at 38 K in the iron arsenide $(Ba_{1-x}K_x)Fe_2As_2$. *Phys. Rev. Lett.* **2008**, *101*, 107006.

(22) Hirschfeld, P. J.; Korshunov, M. M.; Mazin, I. I. Gap symmetry and structure of Fe-based superconductors. *Rep. Prog. Phys.* **2011**, *74*, 124508.

(23) Sefat, A. S. Pressure effects on two superconducting iron-based families. *Rep. Prog. Phys.* **2011**, *74*, 124502.

(24) Alireza, P. L.; Ko, Y. T. C.; Gillett, J.; Petrone, C. M.; Cole, J. M.; Lonzarich, G. G.; Sebastian, S. E. Superconductivity up to 29 K in $SrFe_2As_2$ and $BaFe_2As_2$ at high pressures. *J. Phys.: Condens. Matter* **2009**, *21*, 012208.

(25) Okada, H.; Igawa, K.; Takahashi, H.; Kamihara, Y.; Hirano, M.; Hosono, H.; Matsubayashi, K.; Uwatoko, Y. Superconductivity under high pressure in LaFeAsO. *J. Phys. Soc. Jpn.* **2008**, *77*, 113712.
(26) Kang, J. H.; Xie, L.; Wang, Y.; Lee, H.; Campbell, N.; Jiang, J.; Ryan, P. J.; Keavney, D. J.; Lee, J. W.; Kim, T. H.; Pan, X.; Chen, L. Q.; Hellstrom, E. E.; Rzchowski, M. S.; Liu, Z. K.; Eom, C. B. Control of epitaxial $BaFe_2As_2$ atomic configurations with substrate surface terminations. *Nano Lett.* **2018**, *18*, 6347−6352.
(27) Yin, W. G.; Lee, C.-C.; Ku, W. Unified picture for magnetic correlations in iron-based superconductors. *Phys. Rev. Lett.* **2010**, *105*, 107004.
(28) Tanatar, M. A.; Kreyssig, A.; Nandi, S.; Ni, N.; Bud'Ko, S. L.; Canfield, P. C.; Goldman, A. I.; Prozorov, R. Direct imaging of the structural domains in the iron pnictides AFe_2As_2 (A = Ca,Sr,Ba). *Phys. Rev. B* **2009**, *79*, 180508R.
(29) Rotundu, C. R.; Freelon, B.; Forrest, T. R.; Wilson, S. D.; Valdivia, P. N.; Pinuellas, G.; Kim, A.; Kim, J.-W.; Islam, Z.; Bourret-Courchesne, E.; Phillips, N. E.; Birgeneau, R. J. Heat capacity study of $BaFe_2As_2$: Effects of annealing. *Phys. Rev. B* **2010**, *82*, 144525.
(30) Mani, A.; Ghosh, N.; Paulraj, S.; Bharathi, A.; Sundar, C. S. Pressure-induced superconductivity in $BaFe_2As_2$ single crystal. *EPL* **2009**, *87*, 17004.
(31) Rotter, M.; Tegel, M.; Johrendt, D. Spin-density-wave anomaly at 140 K in the ternary iron arsenide $BaFe_2As_2$. *Phys. Rev. B* **2008**, *78*, 020503R.
(32) Patz, A.; Li, T.; Ran, S.; Fernandes, R. M.; Schmalian, J.; Bud'ko, S. L.; Canfield, P. C.; Perakis, I. E.; Wang, J. Ultrafast observation of critical nematic fluctuations and giant magnetoelastic coupling in iron pnictides. *Nat. Commun.* **2014**, *5*, 3229.
(33) Patz, A.; Li, T.; Luo, L.; Yang, X.; Bud'ko, S.; Canfield, P. C.; Perakis, I. E.; Wang, J. Critical speeding-up of non-equilibrium electronic relaxation near nematic phase transition in unstrained $Ba(Fe_{1-x}Co_x)_2As_2$. *Phys. Rev. B* **2017**, *95*, 165122.
(34) Gati, E.; Xiang, L.; Bud'ko, S. L.; Canfield, P. C. Role of the Fermi surface for the pressure-tuned nematic transition in the $BaFe_2As_2$ family. *Phys. Rev. B* **2019**, *100*, 064512.
(35) Wang, W.; Song, Y.; Cao, C.; Tseng, K.-F.; Keller, T.; Li, Y.; Harriger, L. W.; Tian, W.; Chi, S.; Yu, R.; Nevidomskyy, A. H.; Dai, P. Local orthorhombic lattice distortions in the paramagnetic tetragonal phase of superconducting $NaFe_{1-x}Ni_xAs$. *Nat. Commun.* **2018**, *9*, 3128.
(36) Ge, J. F.; Liu, Z. L.; Liu, C.; Gao, C. L.; Qian, D.; Xue, Q. K.; Liu, Y.; Jia, J. F. Superconductivity above 100 K in single-layer FeSe films on doped $SrTiO_3$. *Nat. Mater.* **2015**, *14*, 285−289.
(37) Lee, J. J.; Schmitt, F. T.; Moore, R. G.; Johnston, S.; Cui, Y. T.; Li, W.; Yi, M.; Liu, Z. K.; Hashimoto, M.; Zhang, Y.; Lu, D. H.; Devereaux, T. P.; Lee, D. H.; Shen, Z. X. Interfacial mode coupling as the origin of the enhancement of T_c in FeSe films on $SrTiO_3$. *Nature* **2014**, *515*, 245−248.
(38) Yang, X.; Vaswani, C.; Sundahl, C.; Mootz, M.; Gagel, P.; Luo, L.; Kang, J. H.; Orth, P. P.; Perakis, I. E.; Eom, C. B.; Wang, J. Terahertz-light quantum tuning of a metastable emergent phase hidden by superconductivity. *Nat. Mater.* **2018**, *17*, 586.
(39) Vaswani, C.; Sundahl, C.; Mootz, M.; Mudiyanselage, D. H.; Kang, J. H.; Yang, X.; Cheng, D.; Huang, C.; Kim, R. H. J.; Liu, Z.; Luo, L.; Perakis, I. E.; Eom, C. B.; Wang, J. Terahertz second harmonic generation from lightwave acceleration of symmetry-breaking nonlinear supercurrents. *Phys. Rev. Lett.* **2020**, *124*, 207003.
(40) Yang, X.; Luo, L.; Mootz, M.; Patz, A.; Bud'ko, S. L.; Canfield, P. C.; Perakis, I. E.; Wang, J. Nonequilibrium pair breaking in $Ba(Fe_{1-x}Co_x)_2As_2$ superconductors: evidence for formation of a photoinduced excitonic state. *Phys. Rev. Lett.* **2018**, *121*, 267001.

https://doi.org/10.1021/acsaelm.2c00291
ACS Appl. Electron. Mater. 2022, 4, 1511−1517